

## **Electronic Supplementary Information**

### **Ultrafast photoinduced dynamics of the organolead trihalide perovskite $\text{CH}_3\text{NH}_3\text{PbI}_3$ on mesoporous $\text{TiO}_2$ scaffolds in the 320-920 nm range**

*Oliver Flender, Johannes R. Klein, Thomas Lenzer,\* and Kawon Oum\**

# 1. Experimental

## 1.1 Preparation and characterization of perovskite samples

Microscope glass slides and quartz substrates (Suprasil I) with a thickness of 1 mm were thoroughly cleaned with acetone and ethanol and then dried at 100 °C. For preparation of the TiO<sub>2</sub> thin films, a mixture of a commercial TiO<sub>2</sub> paste (Dyesol DSL 90T) and 2-propanol (Fisher Scientific, *p.a.*, 99.97%) was prepared (1:9 by volume) and then sonicated for 20 minutes. After doctor blading and a subsequent sintering step at 450 °C, we obtained highly transparent mesoporous TiO<sub>2</sub> films with a thickness of *ca.* 200-300 nm, as estimated from the interference structure of the TiO<sub>2</sub> thin film from the UV into the near-IR region.

Perovskite preparation was carried out in a nitrogen-filled glove-box with a humidity of less than 2%. Three different methods of synthesis were employed:

The 1-step approach was adapted from the prescription of Park, Seok and Grätzel:<sup>1,2</sup> Briefly, a *ca.* 15 wt% “perovskite solution” was prepared by dissolving 220 mg PbI<sub>2</sub> (Sigma Aldrich, 99 %) and 75 mg methylammonium iodide (MAI, Dyenamo) in 1.7 g (1.5 mL)  $\gamma$ -butyrolactone (GBL, Sigma Aldrich,  $\geq$  99%). The solution was stirred for 12 h at 60 °C, passed twice through a filter (0.45  $\mu$ m pore size) and spin-coated for 30 s at 2000 rpm, with an initial loading time of 3 s. Finally, the sample was heated for 5 min at 100 °C on a hotplate.

The 2-step method for perovskite deposition was based on a modified version of the original prescription of Park and Grätzel:<sup>3</sup> Briefly, a solution of 100 mg PbI<sub>2</sub> in 1.0 mL dimethylformamide (DMF, Fisher Scientific, *p.a.*, 99.99%) was spin-coated first for 7 s at 3000 rpm and then for 5 s at 6000 rpm without initial loading time. The substrate was then dried for 10 min at 70 °C and 30 min at 100 °C. Afterwards, a solution of 5 mg MAI in 0.5 mL 2-propanol was spin-coated for 20 s at 4000 rpm after an initial loading time of 20 s, resulting in immediately visible formation of dark-brown perovskite on the mesoporous TiO<sub>2</sub> layer.

A modified version of this 2-step method was employed to obtain samples on TiO<sub>2</sub>/quartz substrates with a lower concentration of perovskite in order to cover the dynamics deeper down into the UV range. Similar to the method of Burschka *et al.*,<sup>4</sup> a solution of 50 mg PbI<sub>2</sub> in 1 mL of DMF was spin-coated (30 s at 500 rpm and 60 s at 2000 rpm) without initial loading time. The sample was heated for 30 min at 70 °C and cooled down. The PbI<sub>2</sub>-coated TiO<sub>2</sub>/glass substrate was dipped into a solution of 200 mg MAI in 20 mL 2-propanol for 20 s and rinsed afterwards. For both 2-step methods, the thin film was finally dried for 30 min at 70 °C and kept under nitrogen overnight.

We note that the 2-step method employing two spin-coating steps (DSDS = Double-Step Double-Spin) provides perovskite layers of slightly better optical quality, *i.e.* showing reduced light scattering and improved homogeneity, compared to samples from 2-step preparation employing consecutive spin- and dip-coating steps (DSSD = Double-Step Spin-Dip), and also compared to the 1-step method described above.

X-ray diffraction (XRD) experiments on CH<sub>3</sub>NH<sub>3</sub>PbI<sub>3</sub>/TiO<sub>2</sub>/glass samples were performed using Cu-radiation ( $K_{\alpha 1} = 1.54060 \text{ \AA}$ ,  $K_{\alpha 2} = 1.54443 \text{ \AA}$ ) on a PANalytical X'Pert MPD PRO diffractometer. The instrument was operated in Bragg-Brentano geometry and equipped with primary and secondary programmable divergence slits set to 8 mm, 0.02 rad primary and secondary soller slits, secondary Ni monochromator and an X'Celerator detector. All samples were mounted on a sample holder PW1812/00 for non-standard samples and measured in a  $2\theta$  range of 5° to 75°

with a step size of  $0.017^\circ$ , a step time of 60 s and a rotation time of the sample of 1 s. A background correction was performed to remove the spectral contribution of the amorphous glass slides.

FTIR spectra were recorded *in-situ* on a Bruker IFS 66v/S spectrometer coupled to a home-built specular reflectance setup. The collimated unpolarized IR output beam was focused on the sample surface by an off-axis paraboloid gold mirror covering angles of incidence in the range  $30\text{-}80^\circ$ . The reflected beam was collimated by a second identical off-axis paraboloid gold mirror. The IR beam was finally focused by a third off-axis paraboloid mirror onto a HgCdTe (MCT) detector. The spectral resolution was  $4\text{ cm}^{-1}$ . The resulting spectra were subjected to a baseline subtraction procedure. For *in-situ* FTIR mapping, the sample was mounted on a piezo x/y translation stage. Spectra were recorded point-by-point for the respective area of interest. The thin films were also inspected in the visible range using an optical microscope (Olympus BX51).

Steady-state absorption spectra of the perovskite samples were recorded on a Varian Cary 5000 dual-beam spectrometer in the range 200-2000 nm. Photoluminescence spectra were measured with an Agilent Cary Eclipse spectrometer.

All steady-state photoluminescence, UV-Vis and FTIR absorption experiments were performed at  $T = 296\text{ K}$  under nitrogen atmosphere.

## 1.2 Pump-Supercontinuum Probe (PSCP) spectroscopy

Ultrafast broadband transient absorption experiments were carried out using our two setups for pump - supercontinuum probe (PSCP) spectroscopy covering the probe wavelength ranges 260-695 nm<sup>5</sup> and 500-920 nm, respectively.<sup>6-11</sup> The perovskite sample was mounted in a home-built, O-ring sealed aluminum cell with a quartz front window. The cell was flushed with a constant flow of nitrogen (purity 4.6) to minimize any influence of water and oxygen. It was attached to a computer-controlled piezo-based x/y translation stage and constantly moved during the experiments in order to expose a fresh sample spot to every single laser shot. Perovskite and  $\text{PbI}_2$  samples were excited through the glass side of the sample either by the second harmonic of the titanium-sapphire amplifier system ( $\lambda_{\text{pump}} = 400\text{ nm}$ ) or a NOPA ( $\lambda_{\text{pump}} = 500$  or  $495\text{ nm}$ ), with a typical pump beam diameter of *ca.* 300  $\mu\text{m}$  and an energy of *ca.*  $0.3\text{ }\mu\text{J pulse}^{-1}$ . The relative polarization between the pump beam and supercontinuum probe beam (diameter *ca.* 120  $\mu\text{m}$ ) was set at magic angle. Chirp-correction was performed with  $\text{TiO}_2/\text{glass}$  or  $\text{TiO}_2/\text{quartz}$  samples. The pump-probe intensity cross-correlation time was *ca.* 90 fs, with a time zero accuracy of *ca.* 10 fs.

## 2. XRD patterns of perovskite samples

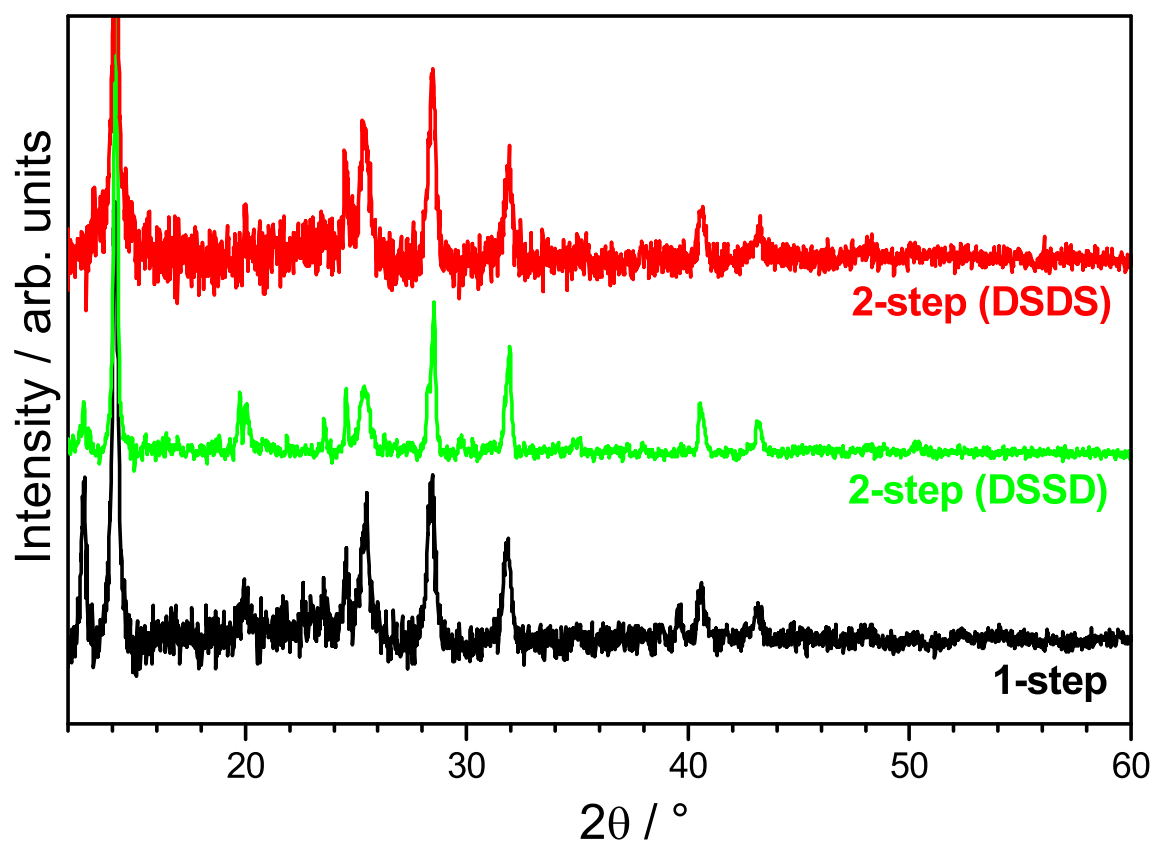


**Fig. S1** XRD patterns of  $\text{CH}_3\text{NH}_3\text{PbI}_3/\text{TiO}_2/\text{glass}$  samples. Perovskite was prepared by different synthesis routes. (Black) 1-step synthesis; (green) 2-step synthesis with spin-coating of  $\text{PbI}_2$  and dip-coating of methylammonium iodide (DSSD); (red) 2-step synthesis with spin-coating of  $\text{PbI}_2$  and spin-coating of methylammonium iodide (DSDS).

### 3. Images from optical microscopy

In **Fig. S2**, we present optical microscopy images of the thin films of mesoporous  $\text{TiO}_2$  nanoparticles, in the presence (upper panels) and absence (lower panels) of organolead trihalide perovskite  $\text{CH}_3\text{NH}_3\text{PbI}_3$ . Each picture (from left to right) represents an image magnified 100-, 200- and 400-fold, respectively. For a comparison, optical microscopy images of uncoated  $\text{TiO}_2$  samples are also presented (lower panels). The recurring patterns in the images result from the instrument background, but not from the thin films.

The perovskite was synthesized by the DSDS method (a detailed description of the synthesis is given in the experimental section above). *Via* this synthetic procedure, thin films of the perovskite material with a high level of homogeneity and good transparency were achieved. Such optical quality of the thin films was indeed advantageous for our laser experiments, providing a reduced level of scattered light, which avoids loss of spectral information near the wavelength of the pump pulse.

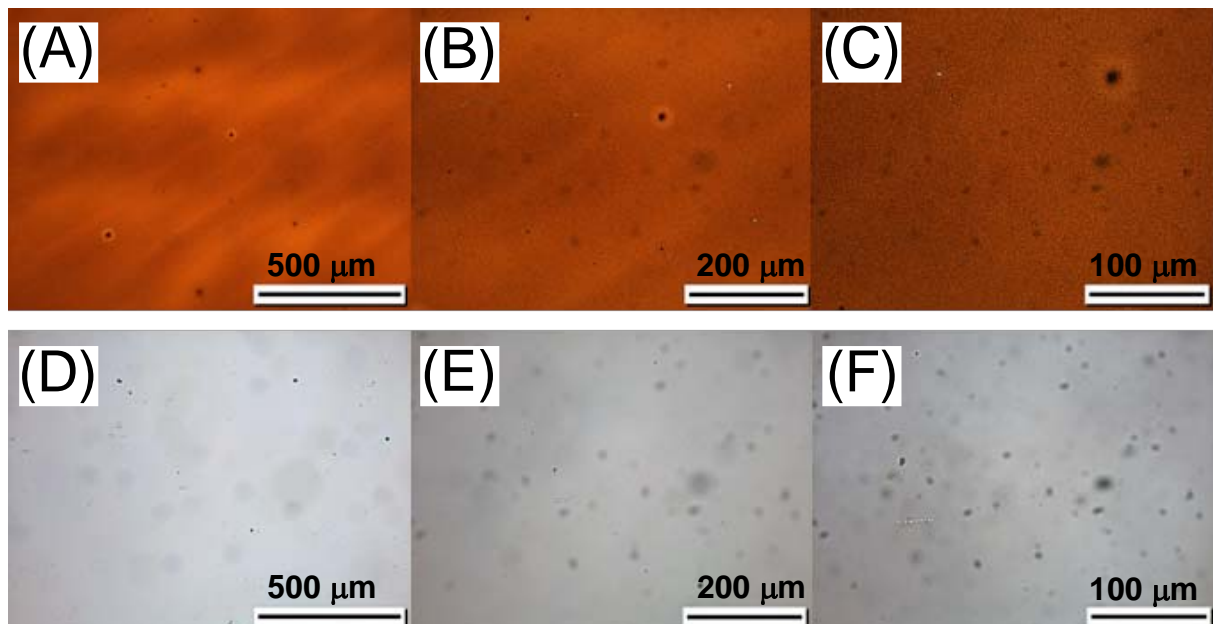


**Fig. S2** Optical microscopy images of the thin films in increasing order of magnification: (upper panels, (A)-(C))  $\text{CH}_3\text{NH}_3\text{PbI}_3$  thin films on mesoporous  $\text{TiO}_2$  nanoparticles; and (lower panels, (D)-(F)) thin films of mesoporous  $\text{TiO}_2$  nanoparticles alone. In all cases, glass substrates were used. The length of each scale bar corresponds to 500 μm for (A) and (D), 200 μm for (B) and (E), and 100 μm for (C) and (F).

## 4. Fits to the Boltzmann tail of the carrier distribution

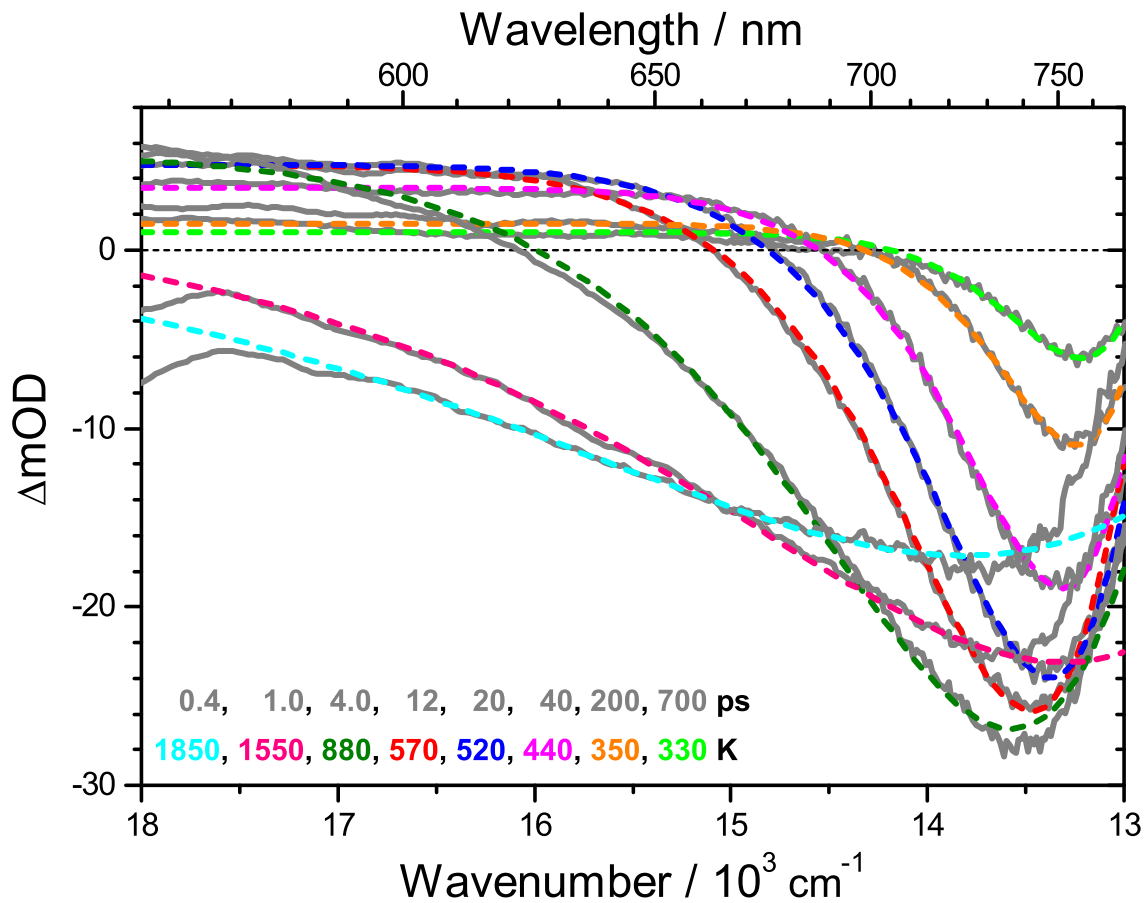


**Fig. S3** Boltzmann fits (dashed colored lines with corresponding temperatures) to selected transient PSCP spectra of  $\text{CH}_3\text{NH}_3\text{PbI}_3$  from Fig. 3 in the time range 0.4-700 ps indicating progressive cooling of the carrier distribution (compare also Fig. 6). The initially broad and extended Boltzmann tail steepens and the distribution narrows upon reduction of the quasi-temperature of the carriers. Note that the loss in signal amplitude, visible from 4 ps onwards, is due to Auger recombination of electrons and holes.

## References:

1. J. H. Heo, S. H. Im, J. H. Noh, T. N. Mandal, C.-S. Lim, J. A. Chang, Y. H. Lee, H.-j. Kim, A. Sarkar, M. K. Nazeeruddin, M. Grätzel and S. I. Seok, *Nature Photon.*, 2013, **7**, 486.
2. J.-H. Im, C.-R. Lee, J.-W. Lee, S.-W. Park and N.-G. Park, *Nanoscale*, 2011, **3**, 4088.
3. J.-H. Im, I.-H. Jang, N. Pellet, M. Grätzel and N.-G. Park, *Nature Nanotech.*, 2014, **9**, 927.
4. J. Burschka, N. Pellet, S.-J. Moon, R. Humphry-Baker, P. Gao, M. K. Nazeeruddin and M. Grätzel, *Nature*, 2013, **499**, 316.
5. K. Oum, T. Lenzer, M. Scholz, D. Y. Jung, O. Sul, B. J. Cho, J. Lange and A. Müller, *J. Phys. Chem. C*, 2014, **118**, 6454.
6. F. Ehlers, M. Scholz, J. Schimpfhauser, J. Bienert, K. Oum and T. Lenzer, *Phys. Chem. Chem. Phys.*, 2015, **17**, 10478.
7. K. Oum, P. W. Lohse, O. Flender, J. R. Klein, M. Scholz, T. Lenzer, J. Du and T. Oekermann, *Phys. Chem. Chem. Phys.*, 2012, **14**, 15429.
8. P. W. Lohse, J. Kuhnt, S. I. Druzhinin, M. Scholz, M. Ekimova, T. Oekermann, T. Lenzer and K. Oum, *Phys. Chem. Chem. Phys.*, 2011, **13**, 19632.
9. K. Golibrzuch, F. Ehlers, M. Scholz, R. Oswald, T. Lenzer, K. Oum, H. Kim and S. Koo, *Phys. Chem. Chem. Phys.*, 2011, **13**, 6340.
10. T. Lenzer, S. Schubert, F. Ehlers, P. W. Lohse, M. Scholz and K. Oum, *Arch. Biochem. Biophys.*, 2009, **483**, 213.
11. A. L. Dobryakov, S. A. Kovalenko, A. Weigel, J. L. Pérez Lustres, J. Lange, A. Müller and N. P. Ernsting, *Rev. Sci. Instrum.*, 2010, **81**, 113106.